

©(2010) Society of Photo-Optical Instrumentation Engineers (SPIE). One print or electronic copy may be made for personal use only. Systematic reproduction and distribution, duplication of any material in this paper for a fee or for commercial purposes, or modification of the content of the paper are prohibited.

Chang, Chein-I., Bharath Ramakrishna, Jing Wang, and Antonio J. Plaza. "Low-Bit Rate Exploitation-Based Lossy Hyperspectral Image Compression." *Journal of Applied Remote Sensing* 4, no. 1 (December 2010): 041760. <https://doi.org/10.1117/1.3530429>.

<https://doi.org/10.1117/1.3530429>

Access to this work was provided by the University of Maryland, Baltimore County (UMBC) ScholarWorks@UMBC digital repository on the Maryland Shared Open Access (MD-SOAR) platform.

### **Please provide feedback**

Please support the ScholarWorks@UMBC repository by emailing [scholarworks-group@umbc.edu](mailto:scholarworks-group@umbc.edu) and telling us what having access to this work means to you and why it's important to you. Thank you.

**Low-bit rate exploitation-based  
lossy hyperspectral image  
compression**

Chein-I Chang  
Bharath Ramakrishna  
Jing Wang  
Antonio Plaza

# Low-bit rate exploitation-based lossy hyperspectral image compression

Chein-I Chang,<sup>a,b</sup> Bharath Ramakrishna,<sup>a</sup> Jing Wang,<sup>a</sup> and Antonio Plaza<sup>c</sup>

<sup>a</sup> University of Maryland, Baltimore County, Department of Computer Science and Electrical Engineering, Remote Sensing Signal and Image Processing Laboratory  
1000 Hilltop Circle, Baltimore, MD 21250 USA  
cchang@umbc.edu

<sup>b</sup> National Chung Hsing University, Department of Electrical Engineering, Taichung, Taiwan

<sup>c</sup> University of Extremadura, Department of Technology of Computers and Communications, Escuela Politecnica de Caceres, Avda. de la Universidad s/n,  
E-10071 Caceres, Extermadura, Spain  
aplaza@unex.es

**Abstract.** Hyperspectral image compression has become increasingly important in data exploitation because of enormous data volumes and high redundancy provided by hundreds of contiguous spectral channels. Since a hyperspectral image can be viewed as a 3-dimensional (3D) image cube, many efforts have been devoted to extending 2D image compression techniques to perform 3D image compression on hyperspectral image cubes. Unfortunately, some major issues generally encountered in hyperspectral data exploitation at low or very low-bit rate compression, for example, subpixels and mixed pixels which do not occur in traditional pure pixel-based image compression are often overlooked in such a 2D-to-3D compression. Accordingly, a direct application of 2D-to-3D compression techniques to hyperspectral image cubes without taking precaution may result in significant loss of crucial spectral information provided by subtle substances such as small objects, anomalies during low bit-rate lossy compression. This paper takes a rather different view by investigating lossy hyperspectral compression from a perspective of exploring spectral information, referred to as exploitation-based lossy compression and further develops spectral/spatial hyperspectral image compression to effectively preserve crucial and vital spectral information of objects which are generally missed by commonly used mean-squared error (MSE) or signal-to-noise ratio (SNR)-based compression techniques when lossy compression is performed at low bit rates. In order to demonstrate advantages of the proposed spectral/spatial compression approach applications of subpixel target detection and mixed pixel analysis are used for experiments for performance evaluation.

**Keywords:** 3D-cube compression, hyperspectral data compression, independent component analysis (ICA), JPEG2000, principal components analysis (PCA), set partitioning in hierarchical tree (SPIHT), spectral/spatial hyperspectral image compression, virtual dimensionality (VD).

## 1 INTRODUCTION

Due to significantly improved spatial and spectral resolution provided by a hyperspectral imaging sensor, hyperspectral imagery expands capability of multispectral imagery in many

ways ranging from subpixel target detection, objection discrimination, mixed pixel classification to material quantification. It also presents new challenges to image analysts, particularly, how to deal with its enormous data volume effectively while still achieving their desired goals. In particular, in many applications such as rare minerals in geology, special spices in agriculture and ecology, toxic waste in environmental monitoring, drug trafficking in law enforcement, combat vehicles in battlefield, abnormalities in intelligent gathering, tumors in medical images etc., the information of interest is generally provided by a target pixel which appears either at so-called subpixel scale in the sense that a subpixel target has size smaller than pixel resolution or as a mixed pixel in a form that fractions of multiple target substances are mixed in a single pixel. In general, such interesting target pixels cannot be identified *a priori* or any prior knowledge due to the fact that the probability of their unexpected occurrence is usually low and their sample population is also relatively small even if they are present. Consequently, the spatial extent of these target pixels is very limited, which results in very little spatial correlation among these target pixels that can be explored by spatial domain-based compression techniques. Accordingly, these types of target pixels may be well likely be sacrificed by spatial domain-based lossy compression if no extra care is taken.

When data compression is performed, two different types of criteria must be specified. One is a design criterion used to develop a compression technique and the other is a performance criterion used to evaluate the effectiveness of a specified compression technique in performance. While these two types of criteria are considered as separate criteria, they are generally correlated to each other. Specifically, a performance criterion is always a major driving force to determine what design criterion should be selected to design a desired compression technique. For example, the Karhunen-Loeve transform (KLT) is the optimal linear transform when the performance criterion is the mean squared error (MSE). On the other hand, when the compression ratio (CR) is used as a performance criterion instead of MSE, the KLT may not be an optimal compression technique in terms of data size reduction. So, how effective a data compression technique is in fact determined by a specific application which in turn determines what a best performance criterion is. This is particularly true for hyperspectral data exploitation where compression performance varies with applications. As examples, in linear spectral mixture analysis for hyperspectral imagery the compression performance should be measured by spectral unmixed error instead of CR or MSE [1]. Similarly, for anomaly detection or endmember extraction the compression performance must be measured by how effectively anomalies or endmembers are extracted rather than CR or MSE. However, it is a common practice in data compression community that CR, MSE, signal-to-noise ratio (SNR) and peak SNR (PSNR) are most widely used criteria in performance analysis. Unfortunately, these criteria may not be effective performance measures in the above-mentioned applications since the targets of interest such as anomalies, endmembers usually do not have many samples in the data set and thus, their contribution to MSE, SNR or PSNR is generally too little to substantiate their existence. Instead, their presence can be only characterized by their spectral properties. To this end, this paper is particularly interested in spectral compression where spectral statistics are used as performance criteria to derive design criteria that can be used to develop compression techniques. Accordingly, the commonly used spectral compression technique, principal components analysis (PCA) can be considered as a 2<sup>nd</sup> order spectral statistics transform which uses data sample variance as a design criterion similar to the MSE used by KLT as a design criterion. By contrast, independent component analysis (ICA) can be regarded as an infinite order statistics-based transform because it uses mutual information as a design criterion to measure statistical independence among independent components it generates. The spectral compression proposed in this paper integrates these component analysis transforms to perform lossy compression for hyperspectral data at low or very low bit rates. In order to address inappropriateness of the commonly used second order statistics-based performance criteria such as MSE and SNR in lossy hyperspectral data compression, several

recent efforts have been focused on criteria going beyond second-order statistics [3-5], for example, a criterion is introduced in [2-3] to include an additional term which is a penalty to non-orthogonality via independent component analysis (ICA) to account for high order statistics and application-oriented performance criteria in [4] such as maximum spectral angle (MSA) and maximum spectral information divergence (SID) with the SID originally proposed in [5] to take into account hyperspectral image classification as applications.

This paper addresses low-bit rate compression problems arising in hyperspectral data by introducing a new concept of exploitation-based hyperspectral data compression where a performance criterion is actually determined by an exploitation-based application instead of an objective measure such as MSE or SNR. In other words, an effective compression performance should be determined by features of objects of interest in data exploitation rather than the data itself such as data size. In many applications, lossless compression may not offer advantages over lossy compression in terms of feature extraction. More specifically, it explores low bit rate exploitation-based hyperspectral data compression where design criteria are derived based on spectral statistics and compression performance is evaluated by selecting an adequate performance criterion to meet a specific goal [6-19]. For example, the principal components analysis (PCA) is a 2<sup>nd</sup> order statistics-based spectral compression technique using data variance as a design criterion. Unfortunately, it was recently shown in [20-21] that another 2<sup>nd</sup> order statistics-based spectral transform, called maximum noise fraction (MNF) or noise adjusted principal component (NAPC) transform which makes use of SNR as a design criterion performs better than PCA when the image quality of multispectral imagery is used as a performance criterion.

It is noted that many unknown and interesting signal sources can be uncovered unknowingly in hyperspectral imagery, such as man-made objects, anomalies that generally provide very important, crucial and vital information for image analysis in defense and intelligence applications. These types of targets give very little attribute to 2<sup>nd</sup> order spectral statistics but can be more effectively characterized by high order spectral statistics such as skewness, kurtosis. If a 2<sup>nd</sup> order statistics-based criterion is used to design an optimal transformation for spectral compression, the compressed data may not be able to capture the spectral characteristics of these targets. Using PCA as an example, these targets may only show in minor components instead of principal components. As a consequence, it will require all PCs to capture these targets rather than preserving only the first few principal components may lose these targets as shown in [19]. Similarly, such targets may be well likely be suppressed by lossy compression techniques which make use of 2<sup>nd</sup> order statistics-based design criteria such as PCA, MNF/NAPC if precaution is not taken. In this case, using high order spectral statistics as design criteria to derive transformations will better serve the purpose of preserving these targets.

For hyperspectral image analysis two types of pixels are of particular interest and are generally not encountered in traditional image processing. One is subpixel targets which are embedded in single pixels and their existence cannot be verified by their spatial properties, but rather specified by their spectral characteristics. The other is mixed pixels which are admixtures of multiple target substances with only partial fractional abundances present in single pixels. In either case, spatial information is not as effective as spectral information. When hyperspectral image compression is performed, it is critical and crucial to take into account this issue which has been unfortunately overlooked by lossy compression in the past. It should be noted that the reason why hyperspectral data is called "hyperspectral" is simply because the spectral information provided by hundreds of contiguous spectral channels is far more important than spatial information in addressing various issues arising in a single pixel vector. In doing so, the exploitation-based hyperspectral image compression introduced in this paper develops a two-stage compression approach, referred to spectral/spatial compression, which performs spectral compression in the first stage followed by spatial compression in the

second stage. It is important to have spectral compression done prior to spatial compression to avoid the spectral information of a single pixel being inadvertently compromised by spatial compression when a 3D compression is directly applied to hyperspectral image cubes as demonstrated by experiments conducted in this paper. Since 3D compression actually performs spectral and spatial compression simultaneously, it is referred in this paper to as 3D-cube compression to reflect the fact that it compresses an image cube as a whole.

One of major techniques to perform spectral compression is dimensionality reduction (DR) by component transforms. The PCA is probably the most widely used component transform to accomplish this goal. However, a key issue for the PCA is determination of the number of principal components needed to be retained after DR for the follow-up spatial compression. A common approach is to calculate the accumulated sum of largest eigenvalues to determine how many components required to be preserved. Unfortunately, it has been shown in [22-23] that such an approach is generally ineffective. Instead, a new concept of the virtual dimensionality (VD) recently introduced in [22-23] was shown to be a better criterion for dimensionality reduction in [24]. On the other hand, it has been also shown in [25-27], the PCA-based spectral compression may not be effective in capturing spectral characteristics exhibited by subpixels and mixed pixels due to the fact that these pixels are more likely to be extracted by high order statistics such as independent component analysis (ICA) [28] rather than second-order statistics based such as variance-based PCA. Therefore, in order to address these two issues, this paper develops various approaches to spectral/spatial compression which include the VD for DR and the use of PCA and/or ICA for spectral compression.

In order to validate the proposed spectral/spatial compression, synthetic images are used and they are custom-designed to simulate various scenarios to demonstrate several interesting findings. Specifically, the experiments show that a direct application of 3D-cube low bit rate lossy compression results in significant loss of spectral information which can be actually preserved by a simple spectral/spatial compression technique. Most importantly, the experimental results also demonstrate that the spectral/spatial compression is more effective than 3D-cube lossy compression in exploitation applications such as subpixel detection and mixed pixel classification/quantification. Additionally, the commonly used SNR and MSE are also shown to be inappropriate compression criteria in hyperspectral image compression when compression ratios are high. To further substantiate simulation results, real hyperspectral image experiments are further conducted for performance analysis and evaluation.

The remainder of this paper is organized as follows. Section II briefly reviews two well-known 2D image compression techniques, wavelet-based JPEG2000 [29-32] and set partitioning in hierarchical tree (SPIHT) [33] along with their extensions to 3D-cube compression. Section III develops several spectral/spatial compression techniques for hyperspectral image compression, which include PCA-based spectral/spatial compression, ICA-based spectral/spatial compression, and mixed (PCA,ICA)-based spectral/spatial compression, all of which use the VD to determine the number of components required to be retained after DR. Section IV custom-designs synthetic images to simulate various scenarios to demonstrate that 3D-cube lossy compression does not necessarily perform better than spectral/spatial compression in subpixel detection and mixed pixel classification. Section V presents real image experiments to further substantiate simulations results. Finally, Section VI concludes with some remarks.

## 2 REVIEW OF 3D COMPRESSION TECHNIQUES

Many 3D-cube image compression techniques are generally extended directly from their 2-D counterparts. Two 3D-cube compression techniques of particular interest that will be used in this paper for comparative study and analysis are the JPEG2000 Multicomponent [32] which is an extension of the wavelet-based 2D-JPEG2000 [29] and the 3D-SPIHT [34-35] which is

extended by 2D-SPIHT developed by Said and Pearlman [33]. It's important to note that in the 3D compression techniques used, the spectral redundancy was reduced by using 1D DWT.

## **2.1 JPEG 2000 multicomponent**

The JPEG2000 [29-30] is a new still image compression standard which has replaced the commonly used DCT-based JPEG. It is a wavelet-based compression technique that adds/improves features such as coding of regions of interest, progressive coding, scalability etc. The entire coding can be divided into four stages: tiling, discrete wavelets transform (DWT), scalar quantization and block coding. The image is divided into rectangular regions called tiles, each tile gets encoded separately. The purpose of dividing images into tiles is that the decoder needs to decode only certain parts of the image on demand, instead of decoding the entire image and also less memory will be needed by the decoder to decode the image. After dividing the image into tiles, a wavelet transform is applied to each tile. The wavelet transform is followed by scalar quantization to quantize the subbands. The scalar quantized subbands representing different scales are coded using Embedded Block Coding with Block Truncation (EBCOT) [29-32,36] scheme. For the case of hyperspectral imagery the Part II of JPEG2000 [32] is implemented to allow multi-component image compression which involves grouping of arbitrary subsets of components into component collections and applying point transforms along the spectral direction like wavelet transform. The post-compression rate-distortion optimizer of EBCOT is simultaneously applied to all codeblocks across all the components.

## **2.2 3D-SPIHT compression**

Recently, an approach developed by Said and Pearlman [33], called set partitioning in hierarchical trees (SPIHT) has become popular. Two main features introduced by Shapiro [37] are used in the SPIHT algorithm. First, it utilizes a partial ordering of coefficients by magnitude and transmits the most significant bits first. Second, the ordering data are not explicitly transmitted. The decoder running the same algorithm can trace the ordering information from the transmitted information. Kim et al [34] later extended the 2D-SPIHT to 3D-SPIHT for video compression in a relatively straightforward manner. There is no constraint imposed on the SPIHT algorithm regarding the dimensionality of the data. If all pixels are lined up in decreasing order of magnitude, 3D-SPIHT performs exactly the same as 2D-SPIHT. In the case of 3D subband structure, one can use a wavelet packet transform to allow a different number of decompositions between the spatial and spectral dimensions.

## **3 SPECTRAL/SPATIAL HYPERSPECTRAL DATA COMPRESSION**

Despite the fact that a hyperspectral image can be viewed as a 3D image cube, there are several major unique features that a hyperspectral image distinguishes itself from being viewed as a 3D image cube. The first and foremost is spectral features provided by hundreds of contiguous spectral channels. Unlike pure voxels in a 3D image, a hyperspectral image pixel vector is specified by a range of wavelengths in a third dimension that characterizes the spectral properties of a single pixel vector. Using the spectral profile captured in the spectral domain a single pixel in a 3D image cube can be solely analyzed by its spectral characterization. Another important unique feature provided by hyperspectral imagery is that many material substances of interest can be only explored by their spectral properties, not spatial properties such as waste in environmental pollution, chemical/biological agent detection in bioterrorism, camouflaged combat vehicles and decoys in surveillance applications. In addition, certain targets such as chemical plumes, biological agents, which are considered to be relatively small with no rigid shapes but yet provide significant information, generally cannot be identified by prior knowledge. Instead, these targets can be only uncovered and revealed by their spectral properties. Therefore, when a compression ratio is high, whether or not a hyperspectral image compression technique is effective may not be necessarily determined by its spatial

compression as do most compression techniques in image processing since small and subtle targets such as subpixel and mixed pixel targets may be very likely sacrificed by low-bit rate compression due to their limited spatial presence. Under such a circumstance, we need count on spectral compression to retain these targets. Accordingly, separating spectral compression from 3D compression may be more desirable and effective than 3D-cube compression compressing spectral and spatial information all together simultaneously in the sense that both the JP2K Part II and 3D-SPIHT codec perform spectral and spatial compression using separable transformations (i.e., 1D linear transform or 1D wavelet packet transform in the spectral dimension and 2D DWT in the spatial dimensions) as a one shot operation. This paper develops an exploitation-based hyperspectral image compression which carries out spectral/spatial compression in a two-stage process where the first stage implements 1D-spectral compression for spectral dimensionality reduction and is then followed by a 3D-cube compression in the second stage. There are key differences between our proposed spectral/spatial compression and 3D-cube compression. One is that our proposed spectral/spatial compression separates spectral compression from spatial compression to perform spectral dimensionality reduction prior to the 3D-cube compression. Another is that after spectral dimensionality reduction our spectral/spatial compression still performs 3D-cube compression on the spectral dimensionality reduced 3D-cube data compared to only 2D spatial compression being performed on the spectral compressed data by 1D spectral compression. A third difference is that there are indeed two types of spectral compression carried out in our proposed spectral/spatial compression, viz. one is spectral dimensionality reduction and the other is spectral redundancy in 3D-cube compression. As a result, two compression criteria can be designed from an exploitation point of view to best fit applications. Finally, a fourth difference is that according to our experience spectral information is better preserved using dimensionality reduction than using 1D wavelet compression since it offers better de-correlation. Accordingly, on many occasions even spectral dimensionality reduction implemented in conjunction with only 2D spatial compression may outperform 3D-cube compression techniques. One such example is the linear spectral mixture analysis (LSMA)-based hyperspectral image compression [1] where the LSMA was used to perform spectral compression by transforming an original hyperspectral image cube to a small number of abundance fractional images that were further processed by a follow-up spatial compression. It is interesting to note that many transform coding methods developed in the literature for hyperspectral image compression generally perform 1D-spectral/2D-spatial compression where a 2D spatial compression technique is applied to individual spectral de-correlated components. However, it has been shown in [25-27] that 1D-spectral/3D-cube compression performed slightly better than 1D-spectral/2D-spatial compression. This is because the former has performed two types of spectral compression, spectral dimensionality reduction by 1D spectral compression followed by spectral redundancy removal by the spectral compression carried out by 1D discrete wavelet in 3D-cube compression as opposed to the latter which is only benefited from 1D spectral dimensionality reduction. As a result, 2D spatial compression is not as effective as 3D-cube compression. Because of that, only techniques for 1D-spectral/3D-cube compression will be used in this paper.

In what follows, we develop various exploitation-based lossy hyperspectral image compression techniques using two component transforms, PCA and ICA to implement 1D-spectral/3D-cube compression where 1D spectral compression is performed by either PCA or ICA as spectral dimensionality reduction and the 3D-cube compression to be used can be one of the two techniques, 3D-multicomponent JPEG2000 and 3D-SPIHT described in Section II.



### 3.1 Principal components analysis (PCA)

The principal components analysis (PCA) is an optimal transform to represent data in the sense of data variance. In transform coding, principal components analysis and Karhunen-Loève transform (KLT) both use the same orthonormal basis to decompose the signal. However, PCA leads to dimension reduction (only principal components are retained), while the KLT retains all the components, as an invertible transform. The idea of PCA can be briefly described as follows.

Assume that  $\{\mathbf{r}_i\}_{i=1}^N$  is a set of  $L$ -dimensional image pixel vectors and  $\boldsymbol{\mu}$  is the mean of the sample pool  $S$  obtained by  $\boldsymbol{\mu} = (1/N) \sum_{i=1}^N \mathbf{r}_i$ . Let  $\mathbf{X}$  be the sample data matrix formed by  $\mathbf{X} = [\mathbf{r}_1 \mathbf{r}_2 \cdots \mathbf{r}_N]$ . Then the sample covariance matrix of the  $S$  is obtained by  $\mathbf{K} = (1/N) [\mathbf{X}\mathbf{X}^T] - \boldsymbol{\mu}\boldsymbol{\mu}^T = (1/N) \left[ \sum_{i=1}^N (\mathbf{r}_i - \boldsymbol{\mu})(\mathbf{r}_i - \boldsymbol{\mu})^T \right]$ . If we further assume that  $\{\lambda_l\}_{l=1}^L$  is the set of eigenvalues obtained from the covariance matrix  $\mathbf{K}$  and  $\{\mathbf{v}_l\}_{l=1}^L$  are their corresponding unit eigenvectors, i.e.,  $\|\mathbf{v}_l\| = 1$ , we can define a diagonal matrix  $\mathbf{D}_\sigma$  with variances  $\{\sigma_l^2\}_{l=1}^L$  and  $\sigma_1^2 \geq \sigma_2^2 \geq \cdots \geq \sigma_L^2$  along the diagonal line as

$$\mathbf{D}_\sigma = \begin{bmatrix} \sigma_1^2 & 0 & \mathbf{0} \\ 0 & \ddots & 0 \\ \mathbf{0} & 0 & \sigma_L^2 \end{bmatrix} \quad (1)$$

and an eigenvector matrix  $\boldsymbol{\Lambda}$  specified by  $\{\mathbf{v}_l\}_{l=1}^L$  as

$$\boldsymbol{\Lambda} = [\mathbf{v}_1 \mathbf{v}_2 \cdots \mathbf{v}_L] \quad (2)$$

such that

$$\mathbf{D}_\sigma = \boldsymbol{\Lambda}^T \mathbf{K} \boldsymbol{\Lambda}. \quad (3)$$

Using the eigenvector matrix  $\boldsymbol{\Lambda}$  a linear transform  $\xi_{\boldsymbol{\Lambda}}$  defined by

$$\xi_{\boldsymbol{\Lambda}}(\mathbf{r}) = \boldsymbol{\Lambda}^T \mathbf{r} \quad (4)$$

transforms every data sample  $\mathbf{r}_i$  to a new data sample,  $\tilde{\mathbf{r}}_i$  by

$$\tilde{\mathbf{r}}_i \equiv \boldsymbol{\Lambda}^T \mathbf{r}_i. \quad (5)$$

As a result, the mean of new  $\xi_{\boldsymbol{\Lambda}}$ -transferred data samples  $\{\tilde{\mathbf{r}}_i\}_{i=1}^N$  becomes  $\tilde{\boldsymbol{\mu}} = (1/N) \sum_{i=1}^N \tilde{\mathbf{r}}_i$  and its resulting covariance matrix is reduced to a diagonal matrix given by

$$\tilde{\mathbf{K}} = (1/N) \sum_{i=1}^N (\tilde{\mathbf{r}}_i - \tilde{\boldsymbol{\mu}})(\tilde{\mathbf{r}}_i - \tilde{\boldsymbol{\mu}})^T = \boldsymbol{\Lambda}^T \mathbf{K} \boldsymbol{\Lambda} = \mathbf{D}_\sigma \quad (6)$$

Equation (6) implies that the  $\xi_{\boldsymbol{\Lambda}}$ -transferred data matrix  $\tilde{\mathbf{X}} = [\tilde{\mathbf{r}}_1 \tilde{\mathbf{r}}_2 \cdots \tilde{\mathbf{r}}_N]$  has been de-correlated or whitened by the matrix  $\boldsymbol{\Lambda}$  which is referred to as a whitening matrix. The transform  $\xi_{\boldsymbol{\Lambda}}$  defined by (5) is an eigen transformation via the eigen matrix  $\boldsymbol{\Lambda}$  and the  $l^{\text{th}}$  component of  $\hat{\mathbf{X}}$  is formed by

$$\xi_{\mathbf{v}_l}(\mathbf{X}) = \mathbf{v}_l^T \mathbf{X} \quad (7)$$

and is called the  $l^{\text{th}}$  principal component (PC) which consists of  $\{\mathbf{v}_l^T \mathbf{r}_i\}_{i=1}^N$  that are  $\xi_{\mathbf{v}_l}$ -transferred data samples corresponding the  $l^{\text{th}}$  eigenvalue  $\lambda_l$ . The PCA is a process that

implements the transform  $\xi_{\mathbf{A}}$  defined by (4) to obtain a set of Principal Components (PCs) via (5) or (7) with all  $1 \leq l \leq L$ . In order to achieve DR, only the PCs specified by eigenvectors that correspond to first  $q$  largest eigenvalues will be retained, while the PCs specified by eigenvectors corresponding to the remaining  $(L-q)$  smaller eigenvalues will be discarded.

### 3.2 Independent component analysis (ICA)

ICA has received considerable interest in recent years to be used to solve blind source separation (BSS) problems because of its versatile applications ranging from source separation, channel equalization to speech recognition and functional magnetic resonance imaging [28]. The idea of BSS is that data are linearly mixed by a set of separate independent sources and demix these signal sources according to their statistical independency measured by mutual information. In order to validate its approach, an underlying assumption is that at most one source in the mixture model can be allowed to be a Gaussian source. This is due to the fact that a linear mixture of Gaussian sources is still a Gaussian source. More precisely, let  $\mathbf{x}$  be a mixed signal source vector expressed by

$$\mathbf{x} = \mathbf{A}\mathbf{s} \quad (8)$$

where  $\mathbf{A}$  is an  $L \times p$  mixing matrix and  $\mathbf{s}$  is a  $p$ -dimensional signal source vector with  $p$  signal sources needed to be separated. The purpose of the BSS is to find a demixing matrix  $\mathbf{W}$  that separates the mixed signal source vector  $\mathbf{x}$  into a set of sources which are statistically the most independent as possible. Several different criteria have been proposed to measure source independency [28]. Nevertheless, they all originated from the concept of mutual information which is a criterion to measure the discrepancy between two random sources.

### 3.3 PCA/3D-cube compression

Using the PCA to de-correlate inter-band spectral information is not new [38-39]. What is new is to use the concept of the VD [22-23] to determine the numbers of PCs required for spectral compression. Since the PCs resulting from the PCA are spectrally de-correlated, we can compress these VD-determined PCs in two ways described in the following two subsections.

#### 3.3.1 PCA/3D-Cube Compression

One way is to form the selected VD-determined PCs as a 3D image cube so that a 3D-cube compression technique can be directly applied for spatial compression. Since the spectral correlation has been compressed by the PCA, a further spatial compression may have little effect on spectral information. The detailed implementation can be summarized as follows.

##### *PCA/3D-Cube Compression Algorithm*

1. Determine the VD of an  $L$ -band hyperspectral image,  $p$ .
2. Form the first  $p$  PCA-generated principal component images as a 3D image cube, referred to as 3D  $p$ -PC image cube.
3. Apply a 3D-cube image compression technique such as 3D-multicomponent JPEG2000 or 3D-SPIHT to the 3D  $p$ -PC image.
4. Exploit the resulting compressed 3D image cube for various applications.

#### 3.3.2 Inverse PCA Image Reconstruction Algorithms

The compression technique described in Section III.A.1 does not reconstruct the image from a compressed image in the original data space formed by the original number of spectral bands. In some applications such as 3D visualization, image reconstruction may be necessary for image analysts. In order to reconstruct a 3D image with the same number of spectral bands of the original hyperspectral image, we can include an additional process which is to apply the inverse of the PCA to reconstruct the original images. The details of implementing IPCA/3D-cube compression can be summarized as follows.

#### *IPCA/3D-Cube Compression Algorithm*

1. Determine the VD of an  $L$ -band hyperspectral image,  $p$ .
2. Form the first  $p$  PCA-generated principal component images as a 3D image cube, referred to as 3D  $p$ -PC image cube.
3. Apply the inverse of the PCA to the spectral dimensionality reduced 3D  $p$ -dimensional PC image cube to reconstruct an image in the original data space.
4. Apply a 3D-cube image compression technique such as 3D-multicomponent JPEG2000 or 3D-SPIHT to the image reconstructed in step 3.
5. Exploit the resulting compressed image obtained in step 4 for various applications.

### **3.4 ICA/3D-cube compression**

The main goal of using the PCA in the previous lossy compression techniques is to perform both dimensionality reduction and spectral de-correlation to achieve data compression. It has been demonstrated in [25-27] that the PCA might not be effective to preserve subtle information that could be only characterized by high-order statistics rather than the second-order statistics such as variance. In order to address this issue, we can use the ICA to replace the PCA in the PCA/3D-cube compression techniques proposed in Sections 3.3. The resulting techniques are referred to as ICA/3D-cube compression techniques. While such PCA  $\leftarrow$  ICA replacement seems intuitive and natural, it is by no means straightforward. One major problem with it is that there is no criterion which can be used to prioritize the components produced by the ICA in the same way that the PCA uses the variance to prioritize its produced PCs. Accordingly, the ICA such as the FastICA developed by Hyvarinen and Oja [40] generally cannot perform dimensionality reduction in the same way that the PCA does. Additionally, the ICA-generated components are statistically independent, not merely second-order de-correlated. Therefore, using the ICA for spectral compression may not be as easy as it was thought.

Recently, the issue of using the ICA for dimensionality reduction was investigated in [24]. Its application to hyperspectral data compression was also explored in [25-27] where three algorithms were developed to rank ICs by different criteria in a similar manner that the PCA does for its PCs using variance as a criterion. Of particular interest is the algorithm that used an unsupervised algorithm, called Automatic Target Generation Process (ATGP) [23,41] to produce an appropriate set of initial projection vectors for the FastICA so that the FastICA-generated ICs can be ranked in the same order that the initial projection vectors generated by the ATGP. This ATGP-FastICA algorithm has been shown to be promising in [24] and will be used in our proposed spectral/3D-cube spatial compression techniques described as follows.

#### **ATGP-FastICA Dimensionality Reduction (ATGP-FastICA DR) Algorithm**

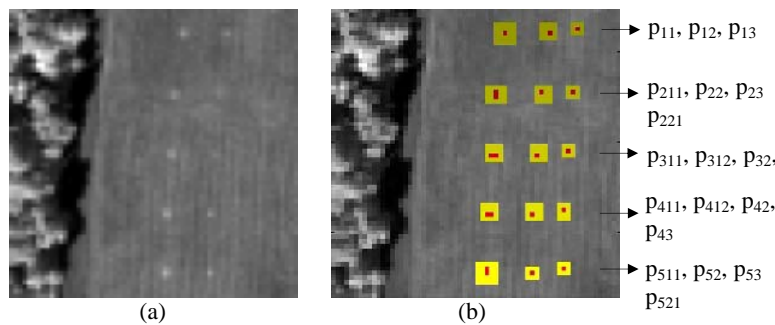
- 1 Use the VD to determine the number of dimensions,  $p$ , required to be retained.  
Perform sphereing on the data matrix  $\mathbf{X}$  and let the resulting sphered data matrix be denoted by  $\hat{\mathbf{X}}$ . It should be noted that the data matrix  $\mathbf{X}$  is formed by grouping all pixel vectors in  $\mathbf{X}$  as column vectors and  $\hat{\mathbf{X}}$  is the data matrix resulting from the sphereing process generally required prior to the FastICA.
- 2 Apply the ATGP to  $\hat{\mathbf{X}}$  to find  $p$  target pixel vector,  $\{\mathbf{t}_i\}_{i=1}^p$ .
- 3 Use the FastICA to find  $p$  independent components,  $\{\mathbf{IC}_i\}_{i=1}^p$  where the  $i$ -th  $\mathbf{IC}_i$  is generated by the FastICA with the  $i$ -th target pixel vector chosen to be the initial projection vector instead of being generated randomly.

By virtue of the ATGP-FastICA DR algorithm described above algorithms similar to PCA/3D-Cube compression algorithm and IPCA/3D-Cube compression algorithm can be further developed by replacing the PCA and IPCA with FastICA and the inverse of the FastICA

respectively, referred to as ICA/3D-Cube compression algorithm and IICA/3D-Cube compression algorithm.

#### 4 SYNTHETIC IMAGE-BASED COMPUTER SIMULATIONS

In order to shed light on the issues of subpixels and mixed pixels in hyperspectral image compression, real hyperspectral image-derived synthetic images were custom-designed to simulate various scenarios to demonstrate facts that blindly applying 3D data compression to a hyperspectral image without extra care may result in significant loss of information. The synthetic images to be used for experiments were simulated from a HYperspectral Digital Image Collection Experiment (HYDICE) image scene in [23]. It is an image scene shown in Fig. 1(a), which has a size of  $64 \times 64$  pixel vectors with 15 panels in the scene and the ground truth map in Fig. 1(b). It was acquired by 210 spectral bands with a spectral coverage from  $0.4\mu\text{m}$  to  $2.5\mu\text{m}$ . Low signal/high noise bands: bands 1-3 and bands 202-210; and water vapor absorption bands: bands 101-112 and bands 137-153 were removed. So, a total of 169 bands were used in experiments. The spatial resolution is  $1.56\text{m}$  and spectral resolution is  $10\text{nm}$ . Within the scene in Fig. 1(a) there is a large grass field background, and a forest on the left edge. Each element in this matrix is a square panel and denoted by  $p_{ij}$  with rows indexed by  $i$  and columns indexed by  $j = 1, 2, 3$ . For each row  $i = 1, 2, \dots, 5$ , there are three panels  $p_{i1}$ ,  $p_{i2}$ ,  $p_{i3}$ , painted by the same paint but with three different sizes. The sizes of the panels in the first, second and third columns are  $3\text{m} \times 3\text{m}$  and  $2\text{m} \times 2\text{m}$  and  $1\text{m} \times 1\text{m}$  respectively. Since the size of the panels in the third column is  $1\text{m} \times 1\text{m}$ , they cannot be seen visually from Fig. 1(a) due to the fact that its size is less than the  $1.56\text{m}$  pixel resolution. For each column  $j = 1, 2, 3$ , the 5 panels have the same size but with five different paints. However, it should be noted that the panels in rows 2 and 3 were made by the same material with two different paints. Similarly, it is also the case for panels in rows 4 and 5. Nevertheless, they were still considered as different panels but our experiments will demonstrate that detecting panels in row 5 (row 4) may also have effect on detection of panels in row 2 (row 3). The  $1.56\text{m}$ -spatial resolution of the image scene suggests that most of the 15 panels are one pixel in size except the panels in the 1<sup>st</sup> column along with the 2<sup>nd</sup>, 3<sup>rd</sup>, 4<sup>th</sup>, 5<sup>th</sup> rows which are two-pixel panels, denoted by  $p_{211}$ ,  $p_{221}$ ,  $p_{311}$ ,  $p_{312}$ ,  $p_{411}$ ,  $p_{412}$ ,  $p_{511}$ ,  $p_{521}$ . Fig. 1(b) shows the precise spatial locations of these 15 panels where red pixels (R pixels) are the panel center pixels and the pixels in yellow (Y pixels) are panel pixels mixed with the background. Fig. 1(c) plots the 5 panel spectral signatures  $\mathbf{p}_i$  for  $i = 1, 2, \dots, 5$  obtained by averaging R pixels in the  $3\text{m} \times 3\text{m}$  and  $2\text{m} \times 2\text{m}$  panels in row  $i$  in Fig. 1(b).



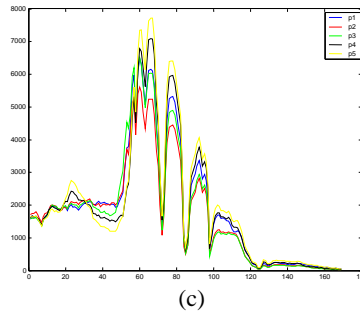


Fig. 1 (a) A HYDICE panel scene which contains 15 panels; (b) Ground truth map of spatial locations of the 15 panels; (c) Spectral signatures of  $p_1$ ,  $p_2$ ,  $p_3$ ,  $p_4$  and  $p_5$

It should be noted the R pixels in the  $1m \times 1m$  panels are not included because they are not pure pixels, mainly due to that fact that the  $1m \times 1m$  panels are smaller than the pixel resolution is 1.56 m. These panel signatures along with the R pixels in the  $3m \times 3m$  and  $2m \times 2m$  panels were used as required prior target knowledge for the following comparative studies. Fig. 1(b) shows the precise spatial locations of these 15 panels where red pixels (R pixels) are the panel center pixels and the pixels in yellow (Y pixels) are panel pixels mixed with the background. The 1.56m-spatial resolution of the image scene suggests that most of the 15 panels are one pixel in size except that  $p_{21}$ ,  $p_{31}$ ,  $p_{41}$ ,  $p_{51}$  which are two-pixel panels. Fig. 1(c) plots the 5 panel spectral signatures  $p_i$  for  $i = 1, 2, \dots, 5$  obtained by averaging R pixels in the  $3m \times 3m$  and  $2m \times 2m$  panels in row  $i$  in Fig. 1(b).

Two popular compression techniques 3D-SPIHT and JPEG2000-Multicomponent are used for benchmark comparison with our proposed exploitation-based spectral/spatial compression techniques. The implementation in QccPack [42] was used for the 3D-SPIHT algorithm. For 3D-SPIHT 4-level spectral and 4-level spatial wavelet packet decomposition was performed. In particular, the wavelet packet decomposition was used instead of the dyadic decomposition because it could be better tailored to the data (the wavelet packet decomposition is considered to be more suitable for hyperspectral images). On other hand, the JPEG2000 algorithm implemented in our experiments was obtained from the kakadu [43] version 4.2.1. Since the kakadu software implements only Part I of the JPEG2000 standard, a 1-D spectral transform was performed separately on the data before feeding the data to the kakadu coder. In order to implement JP2K Part II type compression we applied 1D wavelet transform spectrally using QccPack and the transformed components were then fed to the kakadu codec simultaneously with equal weights given to all components. The codec automatically allocated rate simultaneously across all the components to optimally truncate the embedded bit stream.

All the proposed exploitation-based spectral/spatial compression techniques are carried out in two stages, i.e., VD-determined spectral compression in the 1<sup>st</sup> stage followed by either JPEG2000 Multicomponent or 3D-SPIHT spatial compression in the 2<sup>nd</sup> stage. For the spatial compression, a variable bit-rate lossy compression technique was used in both the JPEG2000 Multicomponent and 3D-SPIHT. More details can be found in [25-27]. The PCA and ICA transforms generate real numbers. We have rounded these numbers to 16 bit in the implementation of spectral/spatial compression techniques. Also the PCA and ICA are data dependent transforms, thus the transformation vectors need to be stored and/or transmitted in order to perform reconstruction of the data, these transformation vectors will act as an overhead, and this overhead factor has been included in the calculation of the compression ratio.

The compression ratios were chosen to be 20, 40, 60 and 100 since little difference was noted in the detection/quantification performance for compression ratios lower than 20. This implied that for very low compression ratios ( $<10$ ) the 3D-cube compression alone and spectral/spatial

based compression can successfully preserve the subpixel and mixed pixel information. Such subtle difference can be only observed when the data are compressed with high compression ratios ( $>40$ ). In order to address the issues of subpixels and mixed pixels, two examples were custom-designed to illustrate and demonstrate the superiority of spectral/spatial compression to the 3D-cube compression in terms of preserving subpixel and mixed pixel spectral information.

The first example was designed to investigate the issue of subpixel quantification of subtle targets (weak signals) embedded in a single background, in which case both PCA and ICA based compression techniques work well as compared to 3D-cube compression alone. As a matter of fact, it was demonstrated in [27] that for subpixel detection of subtle targets (weak signals) over a single background the ICA based compression techniques worked the best. The second example is designed to investigate the issue of subpixel and mixed pixel quantification of strong targets (strong signals) embedded in multiple backgrounds, in which case the ICA cannot be applied and the best results are obtained by using the PCA based compression.

#### Example 1 (Single Background)

The synthetic image to be used for our experiments in this example is shown in Fig. 2 which is similar to the real scene and has the same size of  $64 \times 64$  pixel vectors. The background in the synthetic image was simulated by  $\mathbf{p}_1$  panel signature from the image scene in Fig. 1(c) with an added Gaussian noise to achieve signal-to-noise ratio (SNR) 30:1. There are 16 panels located at the center and arranged in four rows with four panels in each row. The four-pixel panels in the  $i$ -th row and the 1<sup>st</sup> column are composed of single pure pixels, denoted by  $p_{i,11}$ ,  $p_{i,12}$ ,  $p_{i,21}$  and  $p_{i,22}$  pixel vectors simulated by  $\mathbf{p}_{i+1}$  from Fig. 1(b) for  $i = 1, 2, 3, 4$  respectively. The single panel in the  $i$ -th row and the 2<sup>nd</sup> column is a single-pixel panel, denoted by  $p_{i2}$  simulated by  $\mathbf{p}_{i+1}$  with abundance 75%. The single panel in the  $i$ -th row and the 3<sup>rd</sup> columns is a single-pixel panel, denoted by  $p_{i3}$  simulated by  $\mathbf{p}_{i+1}$  with abundance 50%. The single panel in the  $i$ -th row and the 4<sup>th</sup> columns is a single-pixel panel, denoted by  $p_{i4}$  simulated by  $\mathbf{p}_{i+1}$  with abundance 25%. Fig. 2 shows a synthetic image obtained by implanting the 16 simulated panels in the background image where their corresponding background pixels were removed to accommodate the panel pixels. It should be noted that the noise background in Fig. 2 has been visually suppressed because of high intensity gray level values of panel pixels. Table 1 shows the subpixel abundance fractions of the panels in four rows.

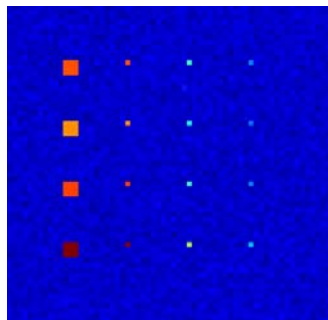


Fig. 2. 16 panels implanted in a single background.

Table 1. The abundance fractions (%) of the panels in four rows.

Panel	$(p_{i,11}, p_{i,12}, p_{i,21}, p_{i,22})$				$(p_{i2})$	$(p_{i3})$	$(p_{i4})$
Pixels	$p_{1,11}$	$p_{1,12}$	$p_{1,21}$	$p_{1,22}$	$P_{12}$	$P_{13}$	$P_{14}$
$\mathbf{p}_2$	100	100	100	100	75	50	25
Pixels	$p_{2,11}$	$p_{2,12}$	$p_{2,21}$	$p_{2,22}$	$P_{22}$	$P_{23}$	$P_{24}$
$\mathbf{p}_3$	100	100	100	100	75	50	25
Pixels	$p_{3,11}$	$p_{3,12}$	$p_{3,21}$	$p_{3,22}$	$P_{32}$	$p_{33}$	$P_{34}$
$\mathbf{P}_4$	100	100	100	100	75	50	25
Pixels	$p_{4,11}$	$p_{4,12}$	$p_{4,21}$	$p_{4,22}$	$P_{42}$	$P_{43}$	$P_{44}$
$\mathbf{P}_5$	100	100	100	100	75	50	25

Clearly, the synthetic image in Fig. 2 is composed of five different classes including four panel signatures  $\mathbf{p}_2$ ,  $\mathbf{p}_3$ ,  $\mathbf{p}_4$ ,  $\mathbf{p}_5$  and one background class  $\mathbf{p}_1$ . To verify this number, a recently developed concept, called virtual dimensionality (VD) in [22-23] was used to determine the number of spectrally distinct signatures present in this synthetic image where a technique, called Harsanyi-Farrand-Chang (HFC) method [44] was used. Table 2 tabulates its VD estimates for the synthetic image Fig. 2 with various false alarm probabilities,  $P_F$ .

Table 2. VD estimates for the synthetic image in Example 1.

$P_F$	$10^{-1}$	$10^{-2}$	$10^{-3}$	$10^{-4}$	$10^{-5}$
VD	5	5	5	5	5

As shown in Table 2, the value estimated by the VD was 5 across all false alarm probabilities, which is exactly the same number of spectrally distinct signatures according to the ground truth. The VD-estimated value, 5 provides the necessary knowledge about how many components needed to be retained when dimensionality reduction is performed, provided that each component can be used to accommodate one distinct signature. In the case of Fig. 2, the number of components required after dimensionality reduction was 5.

In order to demonstrate the issues of subpixels and mixed pixels caused by lossy data compression, the unsupervised fully constrained least squares (UFCLS) developed in [23,45] was used to estimate the abundance fractions of all subpixels and mixed pixels in Fig. 2. Since the results obtained for panels in each of four rows were very similar, Table 3 tabulates the abundance fractions of the 2<sup>nd</sup>, 3<sup>rd</sup> and the 4<sup>th</sup> single pixel panels in the first row of the synthetic image obtained by 3D-cube compression and spectral/3D compression techniques. From Table 3 the performance of 3D SPIHT seemed acceptable for CR = 20, 40, but its performance for CR = 60 and 100 was poor. The performance of JPEG 2000 Multicomponent was very poor in all the cases. On the other hand, our proposed spectral/3D compression techniques except the ICA/ JPEG2000 Multicomponent performed well with all compression ratios where the crucial subpixel and mixed pixel information was well preserved through spectral compression with the spatial compression only causing very little or no deterioration of information provided by subpixels and mixed pixels. In fact, the compression ratios did not seem to have impact on their compression performance. However, despite the fact that the ICA/JPEG2000 Multicomponent did not perform as well as the other three spectral/3D compression techniques did, it was interesting to note that its inverse counterpart, the IICA/JPEG2000 Multicomponent did perform very well. This implied that the ICA/JPEG2000 Multicomponent tended to

overestimate the abundance fractions by over-suppressing the background and the use of inverse ICA-reconstructed images seemed to be able to correct the issue of over-estimated abundance fractions resulting from compression.

Table 3. Abundance fractions (%) for the 2<sup>nd</sup>, 3<sup>rd</sup> and the 4<sup>th</sup> single pixel panels in the first row for different compression ratios

Compression Ratio (CR)	100			60			40			20		
Panels	P <sub>12</sub>	P <sub>13</sub>	P <sub>14</sub>	P <sub>12</sub>	P <sub>13</sub>	P <sub>14</sub>	P <sub>12</sub>	P <sub>13</sub>	P <sub>14</sub>	P <sub>12</sub>	P <sub>13</sub>	P <sub>14</sub>
Original Image	75	50	25	75	50	25	75	50	25	75	50	25
3D – SPIHT	66	39	13	67	47	20	70	50	24	73	50	24
JPEG2000 Multicomponent	61	25	9	67	36	17	70	42	20	71	45	21
PCA/JPEG2000 Multicomponent	75	49	24	75	49	24	75	49	24	75	49	24
ICA/JPEG2000 Multicomponent	75	59	35	75	58	34	75	58	34	75	58	34
IPCA/JPEG2000 Multicomponent	75	49	24	75	49	24	75	49	24	75	49	24
IICA/JPEG2000 Multicomponent	75	49	24	75	49	24	75	49	24	75	49	24

Table 4 also calculated the SNR and MSE for our two proposed spectral/3D compression techniques, IPCA/JPEG2000 Multicomponent and IICA spectral/ JPEG2000 Multicomponent along with 3D-SPIHT, JPEG2000 Multicomponent for CR = 100, 60, 40 and 20. It should be noted that in order to make fair comparison, no MSE and SNR were calculated for PCA/JPEG2000 Multicomponent and ICA/JPEG2000 Multicomponent because they were performed in reduced dimensions.

Table 4. SNR and MSE values for the different compression techniques.

Compression Ratio (CR)	100		60		40		20	
	SNR	MSE	SNR	MSE	SNR	MSE	SNR	MSE
3D - SPIHT	37.65	1.44E+05	37.94	1.35E+05	38.35	1.23E+05	39.53	9.32E+04
JPEG2000 Multicomponent	37.54	1.48E+05	37.80	1.40E+05	38.13	1.29E+05	39.28	9.86E+04
IPCA/JPEG2000 Multicomponent	37.74	1.42E+05	37.74	1.42E+05	37.74	1.42E+05	37.74	1.42E+05
IICA/JPEG2000 Multicomponent	22.41	4.98E+06	22.41	4.98E+06	22.41	4.98E+06	22.41	4.98E+06

As shown in Table 4, the IICA yielded the worst MSE and SNR, but its performance was among the best in terms of subpixel quantification according to Table 3. The reason for this was because the image background was largely suppressed by the ICA and much of background information was lost in the image reconstruction by the IICA.

#### Example 2 (Multiple Backgrounds)

In Example 1, we demonstrated that the JPEG2000 Multicomponent did not perform well for all compression ratios greater than or equal to 20 compared to other techniques, but 3D-SPIHT did reasonably well in some cases such as CR = 20, 40. In the following example, we will further demonstrate that both 3D-SPIHT, JPEG2000 Multicomponent fail to address the issues of subpixels and mixed pixels. In doing so, the synthetic image shown in Fig. 3 was



custom-designed to address the inability of the 3D compression such as 3D-SPIHT and JPEG2000 Multicomponent in preserving quantitative information provided by subpixels and mixed pixels. The image in Fig. 3 is similar to the one used in Example 1 and also has the same size of  $64 \times 64$  pixel vectors.

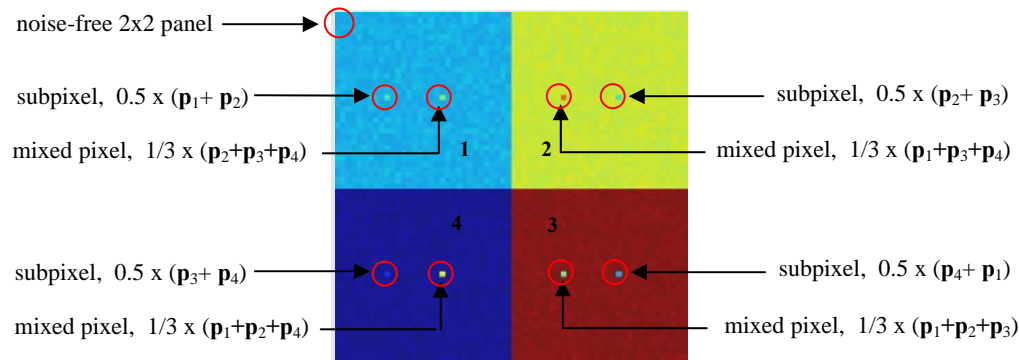


Fig. 3. Synthetic Imagery for Example 2 showing the four quadrants and the subpixel and mixed pixel implanted in each

As shown in Table 2, the value estimated by the VD was 5 across all false alarm probabilities, which is exactly the same number of spectrally distinct signatures according to the ground truth. The VD-estimated value, 5 provides the necessary knowledge about how many components needed to be retained when dimensionality reduction is performed, provided that each component can be used to accommodate one distinct signature. In the case of Fig. 2, the number of components required after dimensionality reduction was 5. The difference between images in Fig. 2 and Fig. 3 is that the image background in Fig. 3 was made up of four different signatures instead of a single image background signature in Fig. 2. First of all, the image was divided into four quarters, each of which had its own background composed of a different panel signature. More specifically, the background in each of the four quarters was simulated by one of  $\mathbf{p}_1$ ,  $\mathbf{p}_2$ ,  $\mathbf{p}_3$ ,  $\mathbf{p}_4$  respectively with an added Gaussian noise to achieve signal-to-noise ratio (SNR) 30:1. The background pixels in a  $2 \times 2$  square panel marked by a circle at the upper left the corner had no noise added.

In each of these quarters a subpixel and a mixed pixel with specific abundance fractions were implanted by replacing the original pixels. There are two single one-pixel panels implanted in each background marked by circles in Fig. 3.

It should be noted that a simulated subpixel target was defined as a target with fractional abundance embedded in a background (B). For example, in the first quadrant the first panel contained a subpixel with target signature  $\mathbf{p}_2$  of fractional abundance 50% with the background signature  $\mathbf{p}_1$  of 50% and the second panel is a mixed pixel with the three signatures  $\mathbf{p}_2$ ,  $\mathbf{p}_3$  and  $\mathbf{p}_4$  sharing the same fractional abundance 1/3.

It is worth noting that this example was particularly designed so that the ICA would not be applicable because the image backgrounds in the four quadrants were simulated by different Gaussian noises, in which case the ICA could not unmix the simulated four Gaussian noises.

Once again, the VD was used to estimate the number of spectrally distinct signatures which was 4 across all false alarm probabilities  $P_F = 10^{-1}$ ,  $10^{-2}$ ,  $10^{-3}$ , and  $10^{-4}$ . The value of 4 estimated by the VD was exactly the same number of panel signatures.  $\mathbf{p}_1$ ,  $\mathbf{p}_2$ ,  $\mathbf{p}_3$ ,  $\mathbf{p}_4$  used to simulate the image in Fig. 3.

Now, the UFCLS was used to estimate the abundance fractions of all subpixels and mixed pixels. Table 5 tabulates the UFCLS-estimated abundance fractions for the subpixel and mixed pixel panels.

Table 5. Abundances fractions (%) for the subpixel and the mixed pixel panels in the first quadrant using UFCLS unmixing [23,45] for different compression ratios.

Panels		Subpixel				Mixed			
CR		100	60	40	20	100	60	40	20
Original	p <sub>1</sub>	50	50	50	50	0	0	0	0
	p <sub>2</sub>	50	50	50	50	33	33	33	33
	p <sub>3</sub>	0	0	0	0	33	33	33	33
	p <sub>4</sub>	0	0	0	0	33	33	33	33
3D - SPIHT	p <sub>1</sub>	70	61	61	55	35	25	25	11
	p <sub>2</sub>	25	36	36	43	11	17	17	24
	p <sub>3</sub>	5	3	3	2	29	31	31	33
	p <sub>4</sub>	0	0	0	0	25	27	27	31
JPEG2000 Multicomponent	p <sub>1</sub>	78	68	68	61	46	20	17	10
	p <sub>2</sub>	8	23	23	33	13	30	31	35
	p <sub>3</sub>	12	7	8	6	23	24	25	26
	p <sub>4</sub>	2	2	1	0	18	26	28	29
PCA/JPEG2000 Multicomponent	p <sub>1</sub>	49	48	48	48	1	1	1	1
	p <sub>2</sub>	45	47	47	47	32	32	32	32
	p <sub>3</sub>	4	4	4	4	34	34	34	34
	p <sub>4</sub>	1	1	1	1	33	33	33	33
IPCA/JPEG2000 Multicomponent	p <sub>1</sub>	49	50	50	50	0	0	0	0
	p <sub>2</sub>	51	50	50	50	33	33	33	33
	p <sub>3</sub>	0	0	0	0	33	33	33	33
	p <sub>4</sub>	0	0	0	0	33	33	33	33

Table 6 also calculated the SNR and MSE for the three compression techniques, 3D-SPIHT, JPEG2000 Multicomponent and IPCA/JPEG2000 Multicomponent with CR = 100, 60, 40 and 20 where all the three produced similar SNRs and MSEs.

Table 6. SNR and MSE values for the different compression techniques.

CR	100		60		40		20	
	SNR	MSE	SNR	MSE	SNR	MSE	SNR	MSE
3D - SPIHT	48.68	1.22E+04	48.98	1.14E+04	49.35	1.05E+04	50.56	7.90E+03
JPEG2000 Multicomponent	48.45	1.28E+04	48.81	1.18E+04	49.13	1.10E+04	50.17	8.64E+03
IPCA/JPEG2000 Multicomponent	48.94	1.15E+04	48.94	1.15E+04	48.94	1.15E+04	48.94	1.15E+04

Apparently, the compression performance of 3D SPIHT and JPEG2000 Multicomponent was very poor for CR = 100 and 60 and only improved slightly even for CR = 40 and 20 in quantification of subpixels and mixed pixels, particularly, their performance in mixed pixel quantification with all compression ratios. By contrast, the IPCA-JPEG2000 Multicomponent and PCA-JPEG2000 with all compression ratios performed consistently better for both subpixel and mixed pixel quantification. The experimental results in this example were also very similar to those in Example 1. According to Tables 5 and 6 the IPCA/JPEG2000 Multicomponent performed very well in both quantification of subpixels and mixed pixels, and

SNR/MSE. Similar conclusions drawn from Examples 1 and 2 were observed in [25-27]. All these experiments conducted in this paper as well as those in [25-27] demonstrated an important fact that using the SNR and MSE as compression measures is inappropriate to address the issues of subpixels and mixed pixels. This implies that the SNR and MSE cannot be blindly applied to hyperspectral data compression without precaution.

## 5 REAL IMAGE EXPERIMENTS

In this section, the real 15-panel HYDICE image scene in Fig. 1 was used for experiments. Similar experiments conducted for the synthetic images in Section IV were also performed for the real image scene in Fig. 1. The CEM [23] and the UFCLS method were also used to investigate the issues of subpixel detection and mixed pixel classification and quantification respectively for the same six compression techniques used in Section IV, 3D-SPIHT, JPEG2000 Multicomponent, PCA/JPEG2000 Multicomponent, ICA/JPEG2000 Multicomponent, IPCA/JPEG2000 Multicomponent and IICA/JPEG2000 Multicomponent for performance evaluation. The VD values estimated by the HFC method for this image scene are tabulated in Table 7 where the VD was empirically selected to be 9 according to experiments in [22-27].

Table 7. VD estimates for the HYDICE image.

$P_F$	$10^{-1}$	$10^{-2}$	$10^{-3}$	$10^{-4}$	$10^{-5}$
VD	14	11	9	9	7

The value of  $VD = 9$  was used to perform dimensionality reduction for our proposed spectral/3D compression.

### Example 3 (Subpixel panel detection)

This example is to demonstrate the effect of lossy compression on target detection in the 15 panels in Fig. 1(b), particularly the five subpixel panels,  $p_{13}$ ,  $p_{23}$ ,  $p_{33}$ ,  $p_{43}$ ,  $p_{53}$  in the 3<sup>rd</sup> column. As the CEM was implemented, the  $p_1$ ,  $p_2$ ,  $p_3$ ,  $p_4$ ,  $p_5$  in Fig. 1(c) were used as desired target signatures. The results of the CEM implemented on the original un-compressed image are shown in Fig. 4.

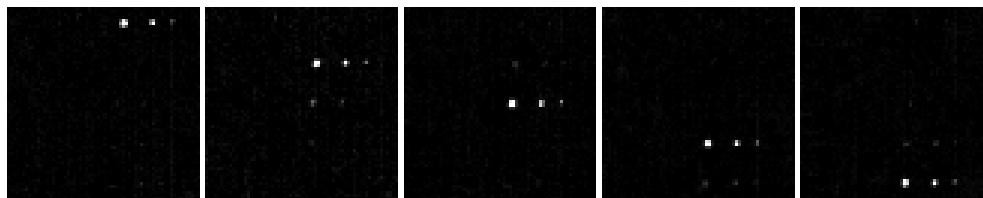


Fig. 4. 15-panel detection results by CEM on the un-compressed original image scene in Fig. 1(a)

Since similar results were obtained for panels in all the five rows, Figs. 5-10 only show results obtained for detection of panels for the 5<sup>th</sup> row by applying the CEM to 6 compressed images resulting from 3D-SPIHT, JPEG2000 Multicomponent, PCA/JPEG2000 Multicomponent, ICA/JPEG2000 Multicomponent, IPCA/JPEG2000 Multicomponent, IICA/JPEG2000 Multicomponent. This was because the detection of the panels in 5<sup>th</sup> row was challenging due to the panels in rows 4 and 5 made by the same panel materials with two different paints. As a result, the CEM detected panels in both rows 4 and 5 if either  $p_4$  or  $p_5$  was used as a desired signature. This was also true for the CEM in detection of panels in the 2<sup>nd</sup> and 3<sup>rd</sup> rows.

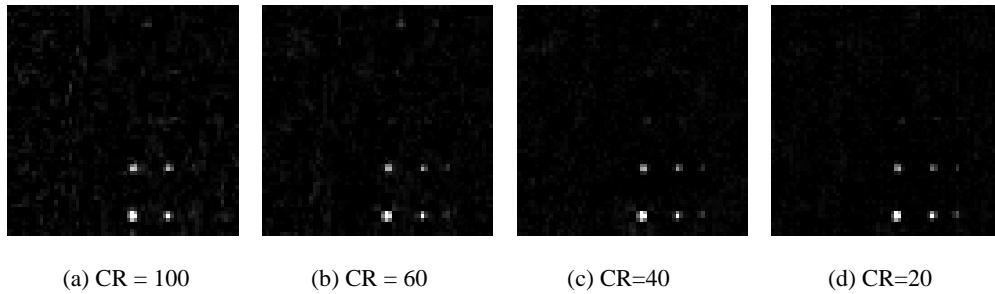


Fig. 5. Detection of panels in 5<sup>th</sup> row by produced by applying CEM to 3D-SPIHT compressed images.

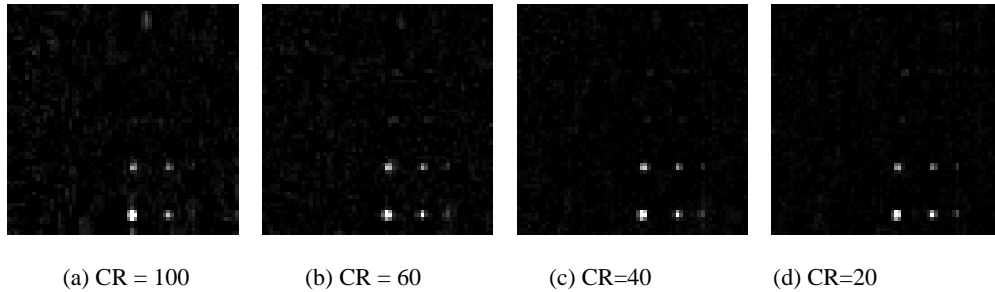


Fig. 6. Detection of panels in 5<sup>th</sup> row by produced by applying CEM to JPEG2000 Multicomponent-compressed images.

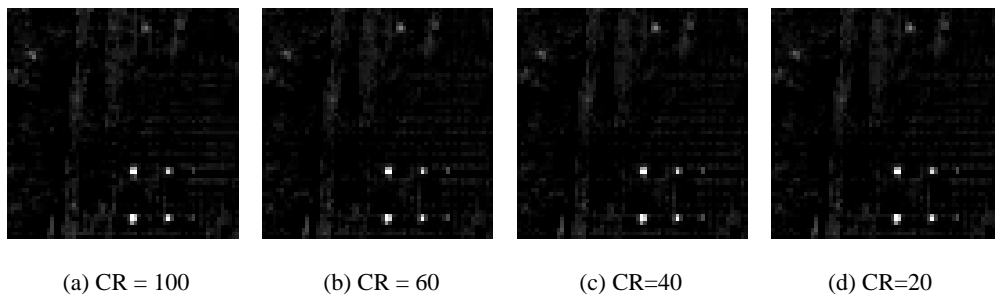


Fig. 7. Detection of panels in 5<sup>th</sup> row by produced by applying CEM to PCA/JPEG2000 Multicomponent compressed images.

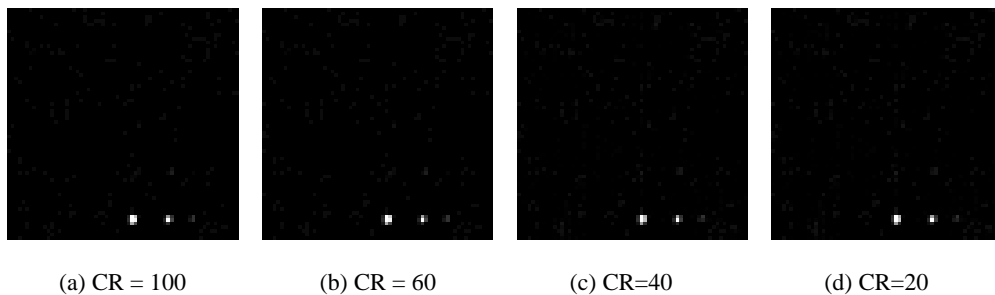


Fig. 8. Detection of panels in 5<sup>th</sup> row produced by applying CEM to ICA/JPEG2000 Multicomponent compressed images.

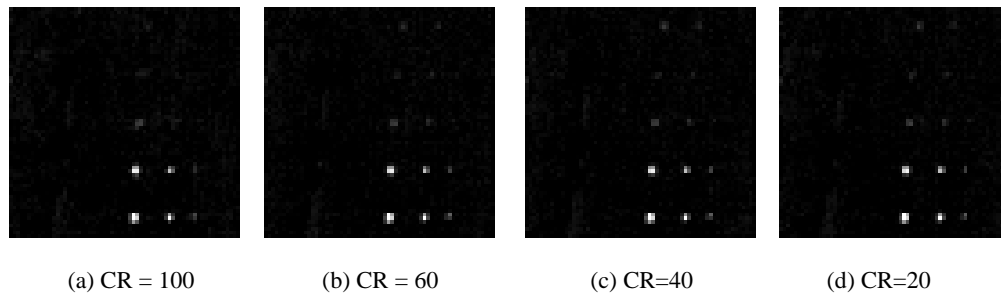


Fig. 9. Detection of panels in 5<sup>th</sup> row by produced by applying CEM to IPCA/JPEG2000 Multicomponent compressed images.

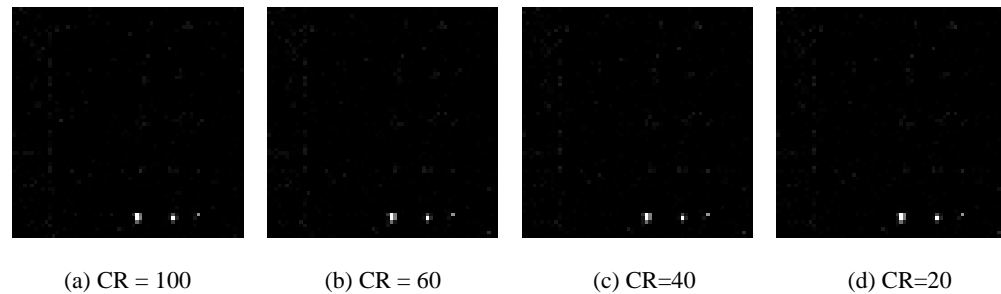


Fig. 10. Detection of panels in 5<sup>th</sup> row by produced by applying CEM to IICA/JPEG2000 Multicomponent compressed images.

Comparing all the detection results in Figs. 5-10 against that in Fig. 4, the best results were those produced by the ICA/JPEG2000 Multicomponent and IICA/JPEG2000 Multicomponent where the PCA-based/3D compression was among the worst and the 3D compression came in between but did not perform well either.

#### Example 4 (Mixed pixel panel quantification)

The experiments conducted in Example 3 were designed to investigate the issue of subpixel target detection where only desired target knowledge was required. This example was conducted to demonstrate the ineffectiveness of 3D lossy compression on mixed pixel panel classification and quantification with the UFCLS used to perform quantification of the 15 panels. In this case, the target knowledge must be known prior to the UFCLS. It was demonstrated in [23,45] that 34 target pixels could be generated in an unsupervised manner and provided sufficient target information for the UFCLS to perform well. Once again, due to similar results that can be obtained for all the 15 panel pixels as Example 3 did, Table 8 only tabulates the UFCLS-estimated abundance fractions (%) of three panels in the 5<sup>th</sup> row where the panel in the 1<sup>st</sup> column is a two-pixel panel, denoted by  $p_{511}$  and  $p_{512}$ , the 2<sup>nd</sup> panel pixel by  $p_{53}$  and the 3<sup>rd</sup> subpanel pixel by  $p_{54}$ . The six lossy compression techniques 3D-SPIHT, JPEG2000 Multicomponent, PCA/JPEG2000 Multicomponent and ICA/JPEG2000 Multicomponent, IPCA/JPEG2000 Multicomponent, IICA/JPEG2000 Multicomponent were evaluated for CR = 100, 60, 40 and 20.

Table 8. Abundance fractions (%) of the mixed pixel panels of the 5<sup>th</sup> row.

CR	100				60				40				20			
	P <sub>511</sub>	P <sub>512</sub>	P <sub>52</sub>	P <sub>53</sub>	P <sub>511</sub>	P <sub>512</sub>	P <sub>52</sub>	P <sub>53</sub>	P <sub>511</sub>	P <sub>512</sub>	P <sub>52</sub>	P <sub>53</sub>	P <sub>511</sub>	P <sub>512</sub>	P <sub>52</sub>	P <sub>53</sub>
Original Image	72	100	78	15	72	100	78	15	72	100	78	15	72	100	78	15
3D - SPIHT	58	100	35	1	55	100	56	8	60	100	62	13	69	100	74	13
JPEG 2000 Multicomponent	57	100	18	0	67	100	48	9	66	100	61	6	62	100	57	11
ICA/JPEG2000 Multicomponent	71	100	70	0	69	100	72	7	69	100	72	12	69	100	72	12
IPCA/JPEG2000 Multicomponent	71	100	77	10	73	100	78	15	72	100	78	18	73	100	78	16
IICA/JPEG2000 Multicomponent	77	100	74	6	67	100	74	8	68	100	75	11	68	100	75	11

From this table we can see that the ICA-based spectral/spatial compression techniques clearly outperformed all other compression techniques. More interestingly, the compression ratios had little effect on the abundance estimates of the PCA/spatial and ICA/spatial compression techniques, while the accuracy of abundance estimates of 3D-SPIHT and 3D-multicomponent JPEG2000 was gradually increased with compression ratios. Finally, Table 9 also tabulates SNR and MSE for the four compression techniques, 3D-SPIHT, JPEG2000 Multicomponent, IPCA/JPEG2000 Multicomponent and IICA/ JPEG2000 Multicomponent with CR = 100, 60, 40 and 20.

Table 9. SNR and MSE for the different compression techniques.

CR	100		60		40		20	
	SNR	MSE	SNR	MSE	SNR	MSE	SNR	MSE
3D-SPIHT	28.38	9.01E+05	31.76	4.13E+05	34.93	1.99E+05	41.10	4.80E+04
JPEG2000 Multicomponent	26.93	1.25E+06	30.02	6.16E+05	32.79	3.26E+05	38.03	9.74E+04
IPCA/JPEG2000 Multicomponent	40.34	5.73E+04	42.52	3.46E+04	42.79	3.26E+04	42.79	3.26E+04
IICA/JPEG2000 Multicomponent	11.66	4.22E+07	11.66	4.23E+07	11.66	4.23E+07	11.66	4.23E+07

As we can see from Table 9, the IICA yielded the worst MSE and SNR, but produced the best detection performance in Fig. 10 among the four techniques. These real image experiments provide further evidence that the MSE and SNR were indeed not appropriate criteria to be used for compression to address issues of subpixels and mixed pixels for hyperspectral image compression.

One particular comment is noteworthy. According to all the experiments conducted in this paper, the improvement on compression performance of the 3D compression techniques was closely related and proportionally to increase of the SNR, decrease of MSE as well as decrease of compression ratio. That is, the better performance a 3D compression, the higher the SNR, the smaller the MSE and the lower the compression ratio. This observation explains the reason why researchers in data compression community have been focused their attention on criteria of SNR and MSE. Unfortunately, this common sense is no longer true for hyperspectral data compression at low bit rates as we demonstrated in our experiments in the above four examples. This is because the SNR and MSE have little impact on subpixel and mixed pixel analysis such as subpxiel detection and mixed pixel quantification when compression ratios are high. In other words, in order for a hyperspectral data compression to be effective, exploitation applications should be considered as the main performance criteria. Blinding using SNR and MSE as compression criteria may have misleading results in hyperspectral data interpretation and analysis.

## 6 CONCLUSION

For a hyperspectral data compression to be effective, hyperspectral data compression must be conducted on an exploitation basis and a blind use of data compression technique generally results in poor performance. Also, a direct application of 3D lossy compression techniques to hyperspectral imagery may cause significant loss of crucial information provided by spectral correlation. It has been shown in this paper by experiments that the SNR and MSE are inappropriate to be used as compression criteria for subpixel and mixed pixel analysis when compression ratios are high. That is, higher SNR or lower MSE does not guarantee better compression performance and vice versa. To address these issues this paper develops spectral/spatial compression techniques which implements a spectral dimensionality reduction transform prior to a 3D compression. Since the spectral dimensionality reduction is performed by component analysis, determining how many components to be retained is very challenging. Over the past years, this number has been assumed *a priori* on a trial and error basis. The proposed spectral/spatial compression uses a newly developed concept of virtual dimensionality (VD) to determine this number. Experimental results demonstrate that such spectral/3D cube compression performs not only better than 3D compression techniques implemented alone, but also better than spectral/2Dspatial compression.

## Acknowledgments

The authors would like to acknowledge the use of the QccPack developed by Dr. J.E. Fowler with the Mississippi State University for the experiments conducted in this work. The authors would also like to acknowledge the use of the Kakadu software developed by Dr. David Taubman. In addition, C.-I Chang would like to thank for support received from the National Science Council in Taiwan under NSC 98-2811-E-005-024 and NSC 98-2221-E-005-096. Last but not least, the authors would like to thank one of anonymous reviewers who went through great details in our paper to provide numerous constructive suggestions which significantly improve our paper quality and presentation.

## Reference

- [1] Q. Du and C.-I Chang, "Linear mixture analysis-based compression for hyperspectral image analysis," *IEEE Trans. Geosci. and Rem. Sens.* **42**(4), 875-891 (2004) [doi:10.1109/TGRS.2003.816668].
- [2] M. Narozy, M. Barret and D.T. Pham, "ICA based algorithms for computing optimal 1-D linear block transforms in variable high-rate source coding," *Signal Process.* **88**(2), 268-283 (2008) [doi:10.1016/j.sigpro.2007.07.017].
- [3] I. P. Akam Bit, M. Barret, and D.T. Pham, "On optimal transforms in lossy compression of multicomponent images with JPEG2000," *Signal Process.* **90**(3), 759-773 (2010) [doi:10.1016/j.sigpro.2009.09.011].
- [4] E. Christophe, D. Leger, and C. Mailhes, "Quality criteria benchmark for hyperspectral imagery," *IEEE Trans. Geosci. and Rem. Sens.* **43**(9), 2103-2114 (2005) [doi:10.1109/TGRS.2005.853931].
- [5] C.-I Chang, "An information theoretic-based approach to spectral variability, similarity and discriminability for hyperspectral image analysis," *IEEE Trans. Inf. Theory*, **46**(5), 1927-1932 (2000) [doi:10.1109/18.857802].
- [6] J. A. Saghr, and A.G. Tescher, "Near-lossless bandwidth compression for radiometric data," *Opt. Eng.* **30**(7), 934-939 (1991) [doi:10.1117/12.55888].
- [7] G. P. Abousleman, E. Gifford, and B. R. Hunt, "Enhancement and compression techniques for hyperspectral data," *Opt. Eng.* **33**(8), 2562-2571 (1994) [doi:10.1117/12.173591].

- [8] G. P. Abousleman, M. W. Marcellin, and B. R. Hunt, "Hyperspectral image compression using entropy-constrained predictive trellis coded quantization," *IEEE Trans. Image Process.* **6**(4), 566-573 (1994) [doi:10.1109/83.563321].
- [9] G. P. Abousleman, M. W. Marcellin and B. R. Hunt, "Compression of hyperspectral imagery using the 3-D DCT and hybrid DPCM/DCT," *IEEE Trans. Geosci. and Rem. Sens.* **33**(1), 26-34 (1994) [doi:10.1109/36.368225].
- [10] V. D. Vaughn and T. S. Wilkinson, "System considerations for multispectral image compression designs," *IEEE Signal Process Mag.* 19-31 (1995) [doi:10.1109/79.363507].
- [11] J. A. Saghri, A. G. Tescher, and J. T. Reagan, "Practical transform coding of multispectral imagery," *IEEE Signal Process Mag.* 32-43 (1995) [doi:10.1109/79.363506].
- [12] S.-E. Qian, A. B. Hollinger, D. Williams, and D. Manak, "Fast three-dimensional data compression of hyperspectral imagery using vector quantization with spectral-feature-based binary coding," *Opt. Eng.* **35**(7), 3242-3249 (1996) [doi:10.1117/1.601062].
- [13] J. A. Saghri, A. G. Tescher, and A. Boujarwah, "Spectral-signature-preserving compression of multispectral data," *Opt. Eng.* **38**(12), 2081-2088 (1999) [doi:10.1117/1.602315].
- [14] M. R. Pickering and M. J. Ryan, "Efficient spectral-spatial compression of hyperspectral data," *IEEE Trans. Geosci. and Rem. Sens.* **39**(7), 1536-1539 (2001) [doi:10.1109/36.934084].
- [15] S.-E. Qian, "Hyperspectral data compression using fast vector quantization algorithm," *IEEE Trans. Geosci. and Rem. Sens.* **42**(8), 65-74 (2004) [doi:10.1109/TGRS.2004.830126].
- [16] Q. Du, W. Zhu, and J. Fowler, "Anomaly-based JPEG2000 compression of hyperspectral imagery," *IEEE Geosci. Remote Sens. Lett.* **5**(4), 696-700 (2004) [doi:10.1109/LGRS.2008.2003180].
- [17] B. Penna, T. Tillo, E. Magli, and G. Olmo, "Progressive 3-D coding of hyperspectral images based on JPEG2000," *IEEE Geosci. Remote Sens. Lett.* **3**(1), 125-129 (2006) [doi:10.1109/LGRS.2005.859942].
- [18] B. Penna, T. Tillo, E. Magli, and G. Olmo, "Transform coding techniques for lossy hyperspectral data compression," *IEEE Trans. Geosci. and Rem. Sens.* **45**(5), 1408-1421 (2007) [doi:10.1109/TGRS.2007.894565].
- [19] Q. Du and J. E. Fowler, "Hyperspectral image compression using JPEG2000 and principal component analysis," *IEEE Geosci. Remote Sens. Lett.* **4**, 201—205 (2007) [doi:10.1109/LGRS.2006.888109].
- [20] A. A. Green, M. Berman, P. Switzer, and M. D. Craig, "A transformation for ordering multispectral data in terms of image quality with implications for noise removal," *IEEE Trans. Geosci. and Rem. Sens.* **26**(1), 65-74 (1988) [doi:10.1109/36.3001].
- [21] J. B. Lee, A. S. Woodyatt, and M. Berman, "Enhancement of high spectral resolution remote sensing data by a noise-adjusted principal components transform," *IEEE Trans. Geosci. and Rem. Sens.* **28**(3), 295-304 (1990) [doi:10.1109/36.54356].
- [22] C.-I Chang and Q. Du, "Estimation of number of spectrally distinct signal sources in hyperspectral imagery," *IEEE Trans. Geosci. and Rem. Sens.* **42**(3), 608-619 (2004) [doi:10.1109/TGRS.2003.819189].
- [23] C.-I Chang, *Hyperspectral Imaging: Techniques for Spectral Detection and Classification*, Kluwer Academic/Plenum Publishers, New York, N.Y. (2003).
- [24] J. Wang and C.-I Chang, "Independent component analysis-based dimensionality reduction with applications in hyperspectral image analysis," *IEEE Trans. Geosci. and Rem. Sens.* **44**(6), 1586-1600 (2006) [doi:10.1109/TGRS.2005.863297].



- [25] B. Ramakrishna, A. Plaza, C.-I Chang, H. Ren, Q. Du, and C.-C. Chang, Spectral/Spatial Hyperspectral Image Compression, *Hyperspectral Data Compression*, edited by G. Motta and J. Storer, Springer-Verlag (2005).
- [26] B. Ramakrishna, "Principal components analysis (PCA)-based spectral/spatial hyperspectral image compression," MS. Thesis, Department of Computer Science and Electrical Engineering, University of Maryland, Baltimore County, Baltimore, MD (2004).
- [27] B. Ramakrishna, J. Wang, A. Plaza and C.-I Chang, "Spectral/spatial hyperspectral image compression in conjunction with virtual dimensionality," *Proc. SPIE* **5806**, Orlando, Florida, 28 March 28-1 April (2005) [doi: 10.1117/12.604128].
- [28] A. Hyvarinen, J. Karhunen, and E. Oja, *Independent Component Analysis*, Wiley, New York (2001).
- [29] D. S. Taubman and M. W. Marcellin, *JPEG2000: Image Compression Fundamentals, Standard and Practice*, Kluwer, Boston, MA (2002).
- [30] J. T. Rucker, J. E. Fowler, and N. H. Younan, "JPEG2000 coding strategies for hyperspectral data," *Proc. Int. Geosci. Rem. Sens. Sym.* **1**, 128–131 (2005) [doi:10.1109/IGARSS.2005.1526121].
- [31] ISO, Information Technology—JPEG 2000 Image Coding System - Part 1: Core Coding System, ISO, Geneva, Switzerland (2000).
- [32] ISO, Information Technology—JPEG 2000 Image Coding System - Part 2: Extensions; Final Committee Draft, ISO, Geneva, Switzerland (2000).
- [33] A. Said and W.A. Pearlman, "A new, fast, and efficient image codec based on set partitioning in hierarchical trees," *IEEE Trans. Circuits Syst. Video Technol.* **6**(3), 243-350 (1996) [doi:10.1109/76.499834].
- [34] B.-J. Kim, Z. Xiong, and W.A. Pearlman, "Low bit-rate scalable video coding with 3-D set partitioning in hierarchical trees (3-D SPIHT)," *IEEE Trans. Circuits Syst. Video Technol.* **10**(8), 1374-1387 (2000) [doi:10.1109/76.889025].
- [35] X. Tang and W. A. Pearlman, "Three-Dimensional Wavelet-Based Compression of Hyperspectral Images," Chapter 10 in *Hyperspectral Data Compression*, Kluwer Academic Publishers, Boston (2005).
- [36] D. Taubman, "High performance scalable image compression with EBCOT *IEEE Trans. Image Process.* **9**(7), 1158-1170 (2000) [doi:10.1109/83.847830].
- [37] J. M. Shapiro, "Embedded image coding using zero trees of wavelet coefficients," *IEEE Trans. Signal Processing*, **41**(12), 3445-3462 (1993) [doi:10.1109/78.258085].
- [38] S. S. Shen and B. S. Beard, "Effects of hyperspectral compression on non-literal exploitation," *Proc. SPIE* **3438**, 191-199 (1998) [doi:10.1117/12.328103].
- [39] A. Kaarna, P. J. Toivanen, and P. Keranen, "Compression of multispectral AVIRIS images," *Proc. SPIE* **4725**, 588-599 (2002) [doi:10.1117/12.478793].
- [40] A. Hyvarinen and E. Oja, "A fast fixed-point for independent component analysis," *Neural Computation*, **9**(7), 1483-1492 (1997) [doi:10.1162/neco.1997.9.7.1483].
- [41] H. Ren and C.-I Chang, "Automatic spectral target recognition in hyperspectral imagery," *IEEE Trans. Aerosp. Electron. Syst.* **39**(4), 1232-1249 (2003) [doi:10.1109/TAES.2003.1261124].
- [42] J. E. Fowler, "QccPack: An open-source software library for quantization, compression, and coding," *Proc. SPIE* **4115**, 249-301 (2000) [doi:10.1117/12.411554].
- [43] Kakadu software: A Comprehensive Framework for JPEG2000, www.kakadusoftware.com, Implementation of JPEG2000.
- [44] J. C. Harsanyi, W. Farrand, and C.-I Chang, "Detection of subpixel spectral signatures in hyperspectral image sequences," *Proc. Am. Soc. Photogramm. Remote Sens. Annu. Mtg.* 236-247 (1994).

- [45] D. Heinz and C.-I Chang, "Fully constrained least squares linear mixture analysis for material quantification in hyperspectral imagery," *IEEE Trans. Geosci. Rem. Sens.* **39**(3), 529-545 (2001) [doi:10.1109/36.911111].

**Chein-I Chang** received his Ph.D. degree in electrical engineering from University of Maryland, College Park and has been with the University of Maryland, Baltimore County since 1987 where he is currently a professor. He is also a chair professor, National Chung Hsing University, Taiwan. Dr. Chang was a plenary speaker for *SPIE Optics+Applications, Remote Sensing Symposium*, 2009 and also a keynote speaker at *2009 Annual Meeting of the Radiological Society of the Republic of China*, Taiwan, *2008 International Symposium on Spectral Sensing Research* in 2008 and *Conference on Computer Vision, Graphics, and Image Processing 2003*, Taiwan. Dr. Chang has authored a book, *Hyperspectral Imaging: Techniques for Spectral Detection and Classification* and edited two books, *Recent Advances in Hyperspectral Signal and Image Processing* and *Hyperspectral Data Exploitation: Theory and Applications*, and co-edited a book on *High Performance Computing in Remote Sensing*. Dr. Chang is a Fellow of SPIE and IEEE.

**Bharath Ramakrishna** is currently a medical imaging scientist at Eigen Inc. He received his BS in Electronics and Communication Engineering from PES Institute of Technology, Bangalore, India in 2002, and his MS and Ph.D. degrees in Computer Engineering from the University of Maryland Baltimore County in 2004 and 2008 respectively. He has authored more than 20 papers comprising of conference proceedings, a book chapter, journal articles. His research interests include image compression, hyperspectral image processing, image segmentation, image registration and computer aided detection. He is a member of Tau Beta Pi, Sigma Xi, SPIE and IEEE.

**Jing Wang** received her BS in electrical engineering and MS degree in computer engineering from the Beijing University of Posts and Telecommunications, Beijing, in 1998 and 2001, respectively, and her Ph.D. degree in electrical engineering from the University of Maryland Baltimore County, Baltimore in 2006. From August 2006 to October 2008, she worked as a research staff in the Xerox Research Center, Webster, NY. Currently, she is working as a senior imaging engineer in Logitech. She is a member of IEEE and SPIE.

**Antonio Plaza** received the M.S. and Ph.D. degrees in computer engineering from the University of Extremadura, Spain in 1997 and 2002 respectively. He was a Visiting Researcher with Remote Sensing Signal and Image Processing Laboratory, University of Maryland Baltimore County; Applied Information Sciences Branch, Goddard Space Flight Center, Greenbelt, MD; and AVIRIS Data Facility, JPL, Pasadena, CA. Since 2000 he has been an Associate Professor with Department of Technology of Computers and Communications, University of Extremadura. He is the Coordinator of the Hyperspectral Imaging Network (Hyper-I-Net), which is a European project designed to build an interdisciplinary research community focused on hyperspectral imaging activities. He is the author or coauthor of more than 150 publications and co-edited a book on high-performance computing in remote sensing and several special issues on remotely sensed hyperspectral imaging for different journals. Dr. Plaza is an Associate Editor for IEEE Transactions on Geoscience And Remote Sensing.